Experimental study of the argumental transverse vibration of a beam excited through permanent or intermittent elastic contact by a harmonic axial motion.

Daniel Cintra, Gwendal Cumunel, Pierre Argoul

Experimental study of the argumental transverse vibration of a beam excited through permanent or intermittent elastic contact by a harmonic axial motion

Daniel Cintra (corresponding author), Gwendal Cumunel
Université Paris-Est,
Laboratoire Navier (UMR 8205), CNRS, ENPC, IFSTTAR,
6 et 8, avenue Blaise Pascal,
Cité Descartes, Champs-sur-Marne,
F-77455 Marne La Vallée Cedex 2, France.
email: daniel.cintra@enpc.fr, gwendal.cumunel@enpc.fr
and
Pierre Argoul
IFSTTAR, Laboratoire MAST-SDOA,
F-77455 Marne La Vallée, Cedex 2, France
email: pierre.argoul@ifsttar.fr

Abstract

The transverse vibration of a beam excited axially by a harmonic motion transmitted through intermittent elastic contact is experimentally studied. The beam's configuration is clamped-(clamped-guided). It is shown that this vibration is in the fundamental transverse mode of the beam, and can occur when the frequency of the excitation is four or six times the frequency of the fundamental transverse mode. The energy transfer between the excitation source and the beam occurs only when the beam is in certain spatial configurations. This constitutes an argumental phenomenon. Experimental results are given and compared to models.

Keywords— nonlinear dynamics; argumental oscillator; beam transverse vibration; axial excitation; spatial modulation; Van der Pol representation.

Contents

1 Introduction.

The so-called argumental oscillator is a mechanical system which has a stable motion consisting of a periodic motion at a frequency next to its natural frequency when submitted to an external force whose frequency is close to a multiple of said natural frequency. One necessary condition for the phenomenon to arise is that the external force be dependent on the space coordinate of the oscillator. An oscillator exhibiting such characteristics has been described in 1928 [1]; this oscillator was a pendulum fitted with a steel sphere at the tip of the rod, submitted to a harmonic magnetic field spatially localized at the bottom of the sphere's course.

The word "argumental" was forged in 1973 [10], where a pendulum is submitted to an electric field spatially localized at the bottom of the pendulum's course.

Further developments were carried out [8, 9], particularly the "multiple resonance" and the "quantum effect". The multiple resonance is a phenomenon in which a number of oscillators, each having its own resonance frequency, submitted to a unique common excitation frequency, can oscillate simultaneously. This is possible if each oscillator has an actual frequency which is a sub-multiple of the excitation frequency, and if the interaction zone between each oscillator and the excitation source is spatially localized. The quantum effect is when an oscillator can oscillate at a number of stable amplitudes whose frequencies are sub-multiples of a fixed excitation frequency. This is possible if the oscillator's actual frequency depends on its amplitude, which is the case for a classical pendulum, and if the excitation source is spatially localized.

Argumental oscillations have also been observed and described in balloon-borne magnetometer measurements [12] and in an electrical circuit [7]. A few examples of argumental oscillators, consisting of six variations of a pendulum excited by magnetic forces, have been modeled and experimented [6]. A stability criterion in symbolic form and an approximate analytic solution for an argumental oscillator have been given [5]. Capture probabilities by an attractor in an argumental oscillator have been given in symbolic form [4].

As for the beams receiving axial excitation, a cantilever beam submitted to a harmonic force through its base and to a pulsating axial force through its tip, and carrying a payload at its tip, has been studied in [11].

A typical second-order ordinary differential equation for a one-degree-of-freedom argumental oscillator is:

$$\ddot{x} + 2\beta\omega_0\dot{x} + \omega_0^2 x = g_1(x) + g_2(x)cos(\omega_{exc}t), \tag{1}$$

where x is the space coordinate, β is the damping ratio, ω_0 is the natural angular velocity of the oscillator, g_1 and g_2 are functions of x, and ω_{exc} is the angular

velocity of the excitation.

The classical averaging calculus makes the hypothesis that the solution has the form $x(t) = a(t)sin(\rho\ \omega_0 t + \varphi(t))$, where $a(t)$ and $\varphi(t)$ are slowly-varying functions of time, "slowly" being with respect to the excitation's signal. This yields the following system, if ρ is chosen so that $n = \dfrac{\omega_{exc}}{\rho\omega_0}$ is an even integer:

$$\begin{cases} \dot{a} &= \dfrac{A(a_A)}{4\rho} S_n(a)\sin(n\varphi) - \beta a \\ \dot{\varphi} &= \dfrac{G(a,a_A)}{\rho a} + \dfrac{A(a_A)}{4\rho a} D_n(a)\cos(n\varphi) - \dfrac{\rho^2-1}{2\rho}, \end{cases} \tag{2}$$

with $A(a_A)$ representing the excitation amplitude a_A, S_n and D_n being two functions of a, G being a function of a and the excitation amplitude a_A.

In this paper, the transverse vibration of a beam excited axially by a harmonic motion transmitted through intermittent elastic contact is experimentally studied. The beam's configuration is clamped-(clamped-guided) (see Fig. 1). It has been shown [3] that this system obeys an argumental equation, and that two models can be devised:

- A discontinuous "natural model", deduced directly from simple physical laws and the arrangement of the constituting components: beam, spring, and points M and A, leading to numerical simulations.
- A continuous "smooth model", approximation to the natural model, allowing a solution using the averaging method [5].

Using experimental results, a comparison is made in this paper with the numerical simulations on the natural model and with the solution provided by the smooth model, using the averaging method. In [2], a few symbolic properties of this system are given.

2 System configuration.

The schematic system configuration is as shown in Fig. 1. A beam is represented, with its left end S and right end M, in a clamped-(clamped-guided) configuration. At the point M's side, the clamp is carried out by way of a massless trolley. Point M is intermittently pushed to the left by a plate C, which is linked to a point A via a massless spring. $\mathbf{F} = F\mathbf{i}$, where $\mathbf{i}$ is the unit vector along the abscissae axis, is the force intermittently applied by plate C to the beam's right end at M. F is negative when the beam is in compression. In the figure, point A moves horizontally with a harmonic motion, in such a manner that the contact between plate C and point M be intermittent when the beam and point A are vibrating. When the beam is in resting (i.e. rectilinear) position and point A is in center position, the force applied to point M is denoted

by F_0.

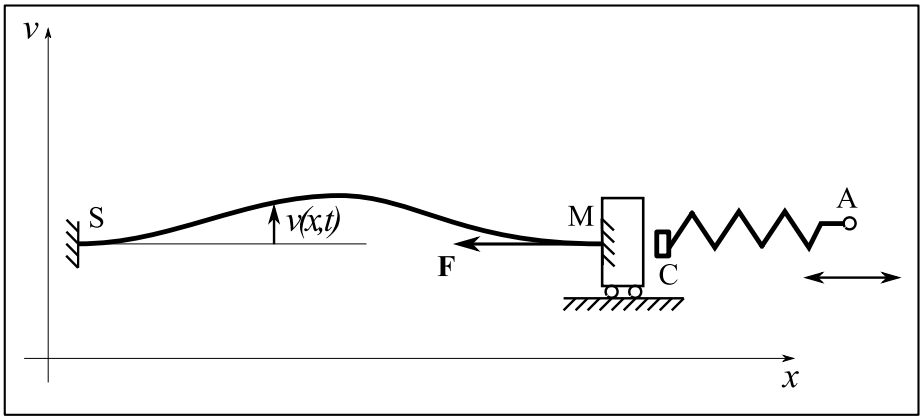

Figure 1: System configuration. x is the horizontal abscissa, v is the transverse displacement, t is the time, and **F** is the force applied by plate C to the beam at point M. Point M moves freely horizontally, but is clamped vertically. There is no rotation at S and M.

Notations:

- ω_{exc} is the angular frequency of the excitation source at point A,
- F_0 is the force F when the beam is at rest and point A is at rest in central position,
- F_B is the beam's critical buckling force,
- ω_0 is the beam's natural angular frequency when point A is at rest in its central position, with $\omega_0^2 = a_1 \left(\frac{\pi}{L}\right)^2 \frac{F_B + F_0}{\mu S}$, where $a_1 = 1$ in the hinged-(hinged-guided) case, and $a_1 = 4/3$ in the clamped-(clamped-clamped) case, μ =mass per volume unit of the beam, S = section of the beam,
- n is an even integer roughly equal to $\frac{\omega_{exc}}{\omega_0}$,
- ρ is a parameter, generally close to 1, chosen so as to have $\frac{\omega_{exc}}{\rho\omega_0} = n$,
- k is the spring's stiffness,
- L is the beam's length,
- $a\,L$ is the amplitude of the beam's motion (a is adimensioned),

- $a_S\ L$ is the amplitude of the beam's stationary-motion (a_S is adimensioned),
- $a_A\ L$ is the amplitude of the excitation at point A (a_A is adimensioned),
- ρ_{00} is defined as $\rho\sqrt{\dfrac{F_B}{F_B+F_0}}$,
- β is the experimentally-measured beam's damping ratio,
- A is a function of a_A characterizing the excitation amplitude,
- S_n and D_n are two functions of a characterizing the spectral components of the interaction between the BUT and the external excitation,
- G is a function of a and a_A characterizing the spatial localization of the interaction between the BUT and the external excitation.

3 Experimental setup.

Define n the frequency ratio of the excitation frequency to the beam's transverse motion frequency. In this section, the experimental setup which has been used to test the cases $n = 4$ and $n = 6$ is presented, along with its calibration procedure.

3.1 Description.

To implement the arrangement shown in Fig. 1, a "beam under test" (BUT) is placed at the left-hand of the experimental setup, while the spring and point A of Fig. 1 are embodied by a second beam, called "control beam", which is excited transversally by a shaker (see Fig. 2). The point A of Fig. 1 is embodied by the junction point between the control beam and the shaker's rod, while the spring of Fig. 1 is embodied by the control beam. Thus, the elasticity of the spring is embodied by the bending elasticity of the control beam. Although the bending elasticity of the control beam is not strictly constant, the experiments and calibrations show that it can be considered constant over the displacement range of the shaker for the experiments which were carried out. Both beams are made of aluminum. The boundary conditions of the BUT are: clamped at the left end and clamped-guided at the right end, where the translational joint is achieved by means of two thin spring steel strips (0,4 mm thickness), as seen in Fig. 3, in a parallelogram configuration allowing the translation of the beam attached to them. As for the control beam, the left end is a clamped-guided joint and the right end is a decentered revolute joint. The decentered revolute joint consists of a cylinder, the circumference of which the end of the beam is attached to, and of two bearings, as illustrated in Fig. 4. To minimize the rotation at the left end of the control beam, due to its small length, the distance between the strips is increased, compared to the configuration of the right end

of the BUT (see Fig. 3).
In order to limit the occurrence of high-frequency modes of the BUT, its first resonance frequency is lowered by addition of local masses. Stiffeners are added to isolate the first mode by pushing aside the higher modes. The same procedure is done on the control beam. A steel ball is machined and glued on the edge of the BUT so as to provide a punctual (sphere-plane) contact between the two beams. To adjust the intermittent contact of the two beams, allowing the occurrence of the researched phenomenon, a steel spring strip (thickness of 0,1 to 0,3 mm) can be added, if necessary, between the ball and the control beam (see Fig. 3).
The measurements are carried out by two laser displacement sensors (Keyence IL-030, around $1\mu m$ resolution, time step of 0,33 ms): one near the left end of the BUT to measure its deflection (see Fig. 5), and the other one, located near the center of the control beam and in front of the shaker, to measure the deflection of the control beam. The shaker (Modalshop model 2004E), driven by a power amplifier (B&K 2719), is used to transversally excite the control beam. The connection between the shaker and the beam is made by way of a centered revolute joint (see Fig. 6).
As the position of point A of Fig. 1 must be precisely commanded, the shaker's position is controlled by a feedback loop. The global synoptic diagram is in Fig. 7. A CompactRIO controller (NI 9076) with two CompactDAQ modules (NI 9234 for the measurements acquisition and NI 9263 for the excitation signal generation) is used to carry out the active control of the shaker. Except for the feedback-control part of this diagram, the system's principle and logic implementation is the same as described in [6].

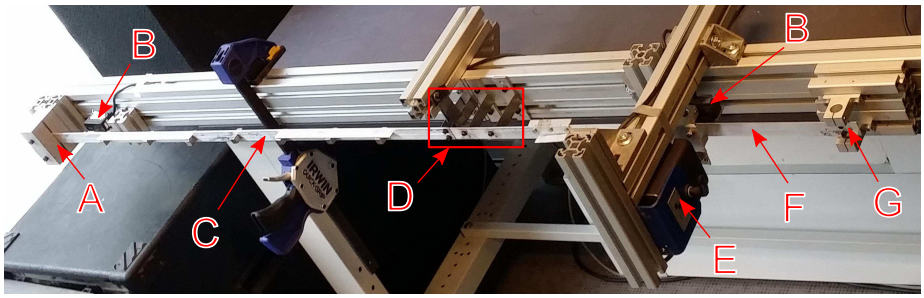

Figure 2: Experiment's global view. A: clamped joint, B: position sensor, C: beam under test (BUT), D: spring steel strips region (detailed in Fig. 3), E: shaker, F: control beam, G: decentered revolute joint.

Remark. In this paper, the experiments are made with two beams so arranged that the head of the control beam has a motion frequency the same as the control beam's transverse motion, because the control beam's position at rest is offset from the rectilinear position (see Fig. 8).

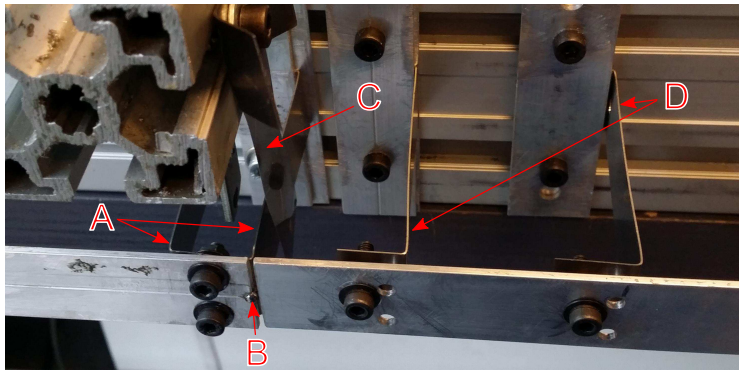

Figure 3: Contact point's environment. A: spring steel strips of the beam under test (BUT), B: steel ball at the contact point between the two beams, C: contact-adjustment spring steel strip, D: spring steel strips of the control beam.

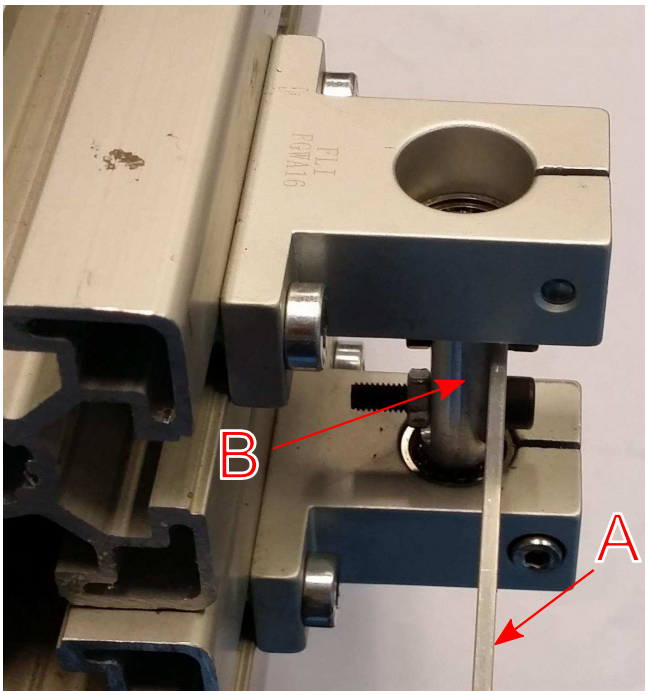

Figure 4: Control beam's pivot joint. A: control beam, B: decentered revolute joint.

3.2 Spectral-purity monitoring.

To ensure that the shaker does not introduce signals into the beam under test (BUT) which induce a classical resonance of the BUT, the spectral contents

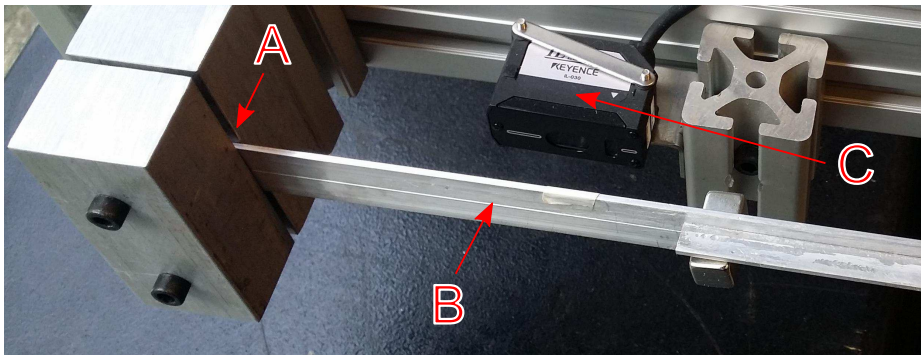

Figure 5: BUT's deflection measurement. A: clamped joint, B: BUT, C: position sensor.

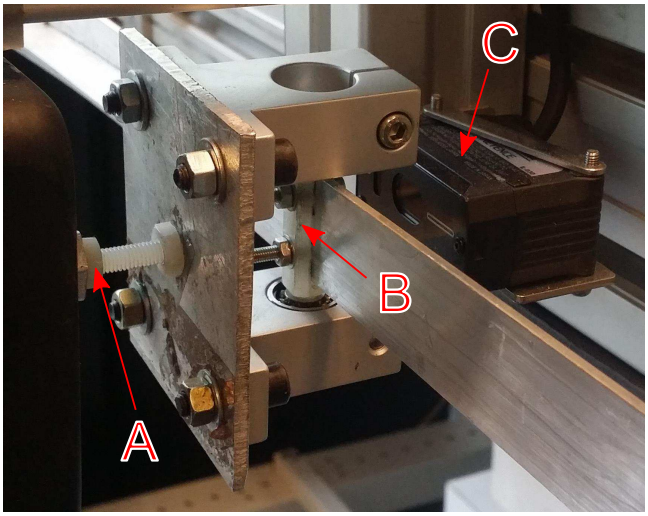

Figure 6: Shaker. A: nylon rod and nuts, B: axis of the revolute joint, C: control beam's position sensor.

of the motion of point A must be monitored. As only the first mode of the BUT is considered in this paper, the classical beam resonance of said first mode arises when point A's frequency is twice the BUT's resonant frequency f_0. So, measurements of the amplitudes of point A's motion and the corresponding transverse motion of the BUT have been carried out at an excitation frequency of $2f_0$. Moreover, the frequency f_0 has been investigated too. The results are in Table 1. Point A's peak-to-peak amplitude (in mm) versus the shaker's peak-to-peak amplitude (in mm) is obtained from the data in Fig. 9, which yield a slope of $0.04mm/mm$. One must then divide by 2 to obtain the classical amplitude from the peak-to-peak amplitude. The BUT's adimensioned amplitude

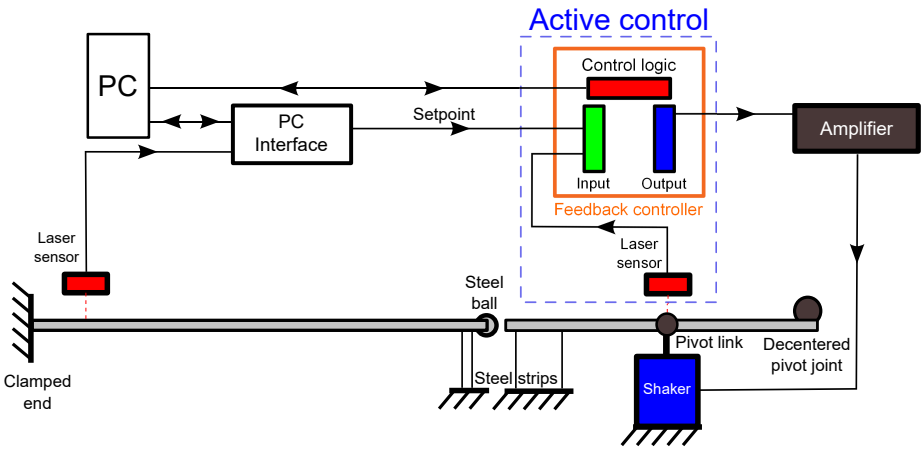

Figure 7: Global synoptic diagram.

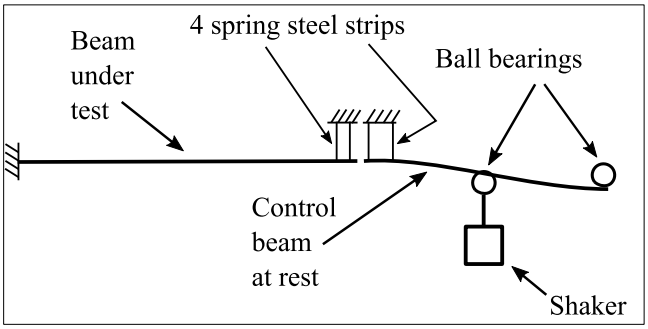

Figure 8: Offset position of the control beam at rest.

(in mm/m) is obtained by dividing the BUT's amplitude (in mm) by L, where L is the length of the BUT. The values of the shaker's spectrum components are in arbitrary unit of power.

It can be seen that if the shaker's unwanted power spectrum components corresponding to the frequencies f_0 and 2 f_0 are kept under 3.5 10^{-5}, then the corresponding unwanted BUT amplitudes are kept under $0.063mm/m = 0.063\ 10^{-3}$. The hypothesis is herein made, that the order of magnitude of the BUT's response due to these unwanted components at f_0 and 2 f_0 is still valid when these components are mixed with high-amplitude components at 4 f_0 or 6 f_0 during the experiments.

Table 1: Amplitude of the BUT's transverse motion in response to axial excitations at f_0 and $2f_0$, for various amplitudes of point A, f_0 being the BUT's resonant frequency.

Shaker's and point A's frequency	Shaker's pk-pk amplitude (mm)	Point A's amplitude (mm)	Beam's amplitude (mm/m)	Shaker's Power spectrum component
f_0	0.62	0.012	1.2	$20\ 10^{-3}$
f_0	0.38	0.0076	0.99	$8.3\ 10^{-3}$
f_0	0.19	0.0037	0.28	$1.8\ 10^{-3}$
f_0	0.024	0.00048	0.039	$1.9\ 10^{-5}$
f_0	0.012	0.00024	0.024	$1.8\ 10^{-6}$
$2\ f_0$	0.57	0.011	1.4	$5.1\ 10^{-3}$
$2\ f_0$	0.19	0.0038	0.47	$5.6\ 10^{-3}$
$2\ f_0$	0.09	0.0018	0.19	$1.3\ 10^{-3}$
$2\ f_0$	0.015	0.0003	0.063	$3.5\ 10^{-5}$
$2\ f_0$	0.005	0.0001	0.009	$3.9\ 10^{-6}$

3.3 Calibration for the case $n = 4$.

Due to the very small displacements at the contact point between the BUT and the control beam, the position of the tip of the control beam has to be derived from its transverse displacement, and therefore a calibration has to be made.
First, the static position of point A is measured as a function of the shaker's static position, given by a position sensor. To do this, the resonant frequency of the BUT is measured for various thicknesses of spring steel strips inserted between the two beams; by comparing the frequencies, it is possible to establish reference points and to determine, step by step, the points of Fig. 9. Then, by measuring the resonant frequency under various static positions of the shaker, an empirical relation between the static position of point A and the static axial force F_0 can be established. The results are given in Fig. 10. Then, by taking the numerical derivative of F_0 with respect to x_A, the local value of the stiffness k is obtained. The results are given in Fig. 11. Finally, the value of the stiffness k retained for the experiment is obtained using a value of k obtained in the region corresponding to the mean value of x_A of this figure. The value retained for k is $k = 200\ kN/m$.

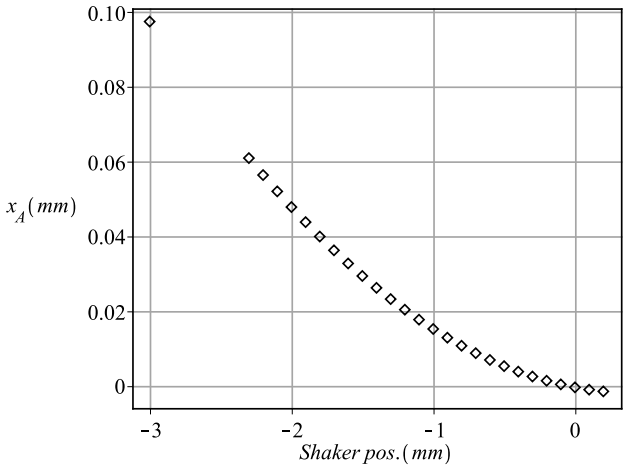

Figure 9: Point A's peak-to-peak amplitude against shaker's peak-to-peak amplitude for the case $n = 4$, with contact adjustment carried out by adding a $0.1mm$ spring steel strip in the experiments. Measured points are represented as diamonds.

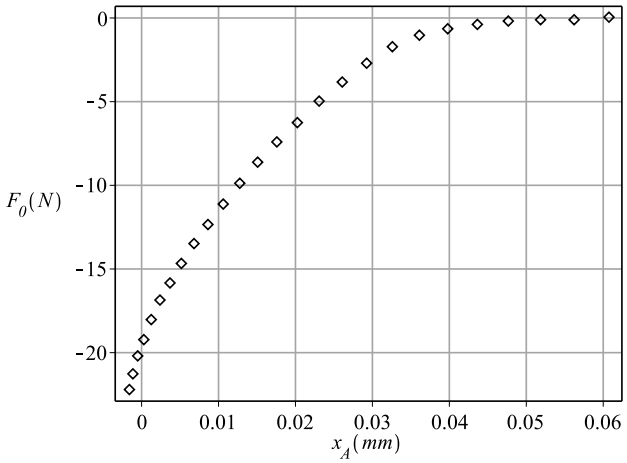

Figure 10: Static axial force F_0 against point A's static position for the case $n = 4$, with contact adjustment carried out by adding a $0.1mm$ spring steel strip in the experiments. Measured points are represented as diamonds.

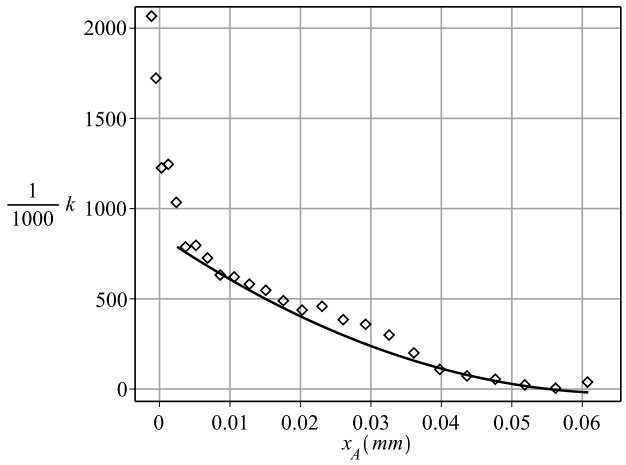

Figure 11: Stiffness k against point A's static position for the case $n = 4$, and trend curve in the region of interest (solid line), with contact adjustment carried out by adding a $0.1mm$ spring steel strip in the experiments. Measured points are represented as diamonds.

3.4 Calibration for the case $n = 6$.

For the case $n = 6$, it was necessary to add a stiffener on the control beam to avoid a mode between point C and the shaker head. So the value of k changed, as well as the relationship between the shaker's position and x_A. The value retained for k is now $k = 130\ kN/m$. The calibration procedure is the same as for the case $n = 4$.

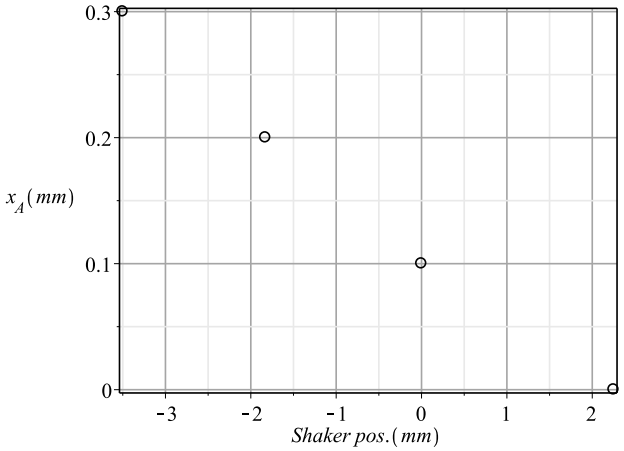

Figure 12: Point A's static position against shaker's static position for the case $n = 6$, with contact adjustment carried out by adding a $0.1mm$ spring steel strip in the experiments. Measured points are represented as circles.

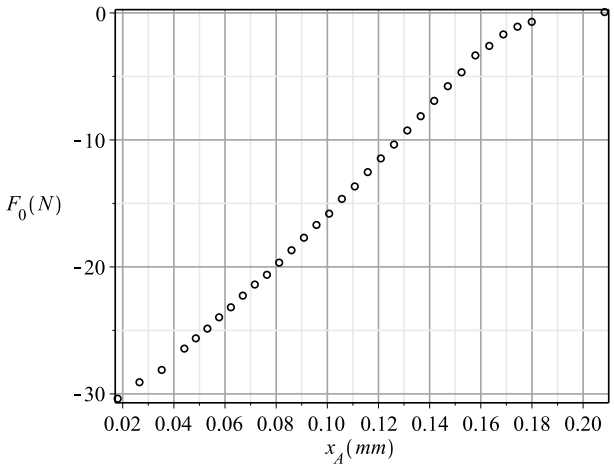

Figure 13: Static axial force F_0 against point A's static position for the case $n = 6$, with contact adjustment carried out by adding a $0.1mm$ spring steel strip in the experiments. Measured points are represented as circles.

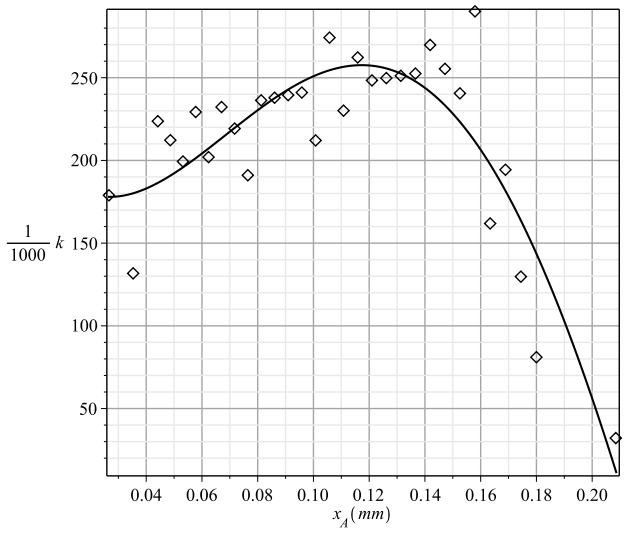

Figure 14: Stiffness k against point A's static position for the case $n = 6$, and trend curve (solid line), with contact adjustment carried out by adding a $0.1mm$ spring steel strip in the experiments. Measured points are represented as diamonds.

4 Experimental results.

In this section, the experimental results are presented in Van der Pol plots, along with other detailed data about the motion and spectral purity. Those Van der Pol plots are polar plots with a as modulus and φ as argument, with reference to Equ. (2). The damping ratio β has been determined experimentally.

4.1 Frequency ratio: $n = 4$

Fig. 15 shows the experimental Van der Pol curves obtained with a frequency ratio $n = 4$. Fig. 16 shows the detail of one curve from Fig. 15. This curve lasted for $40s$.

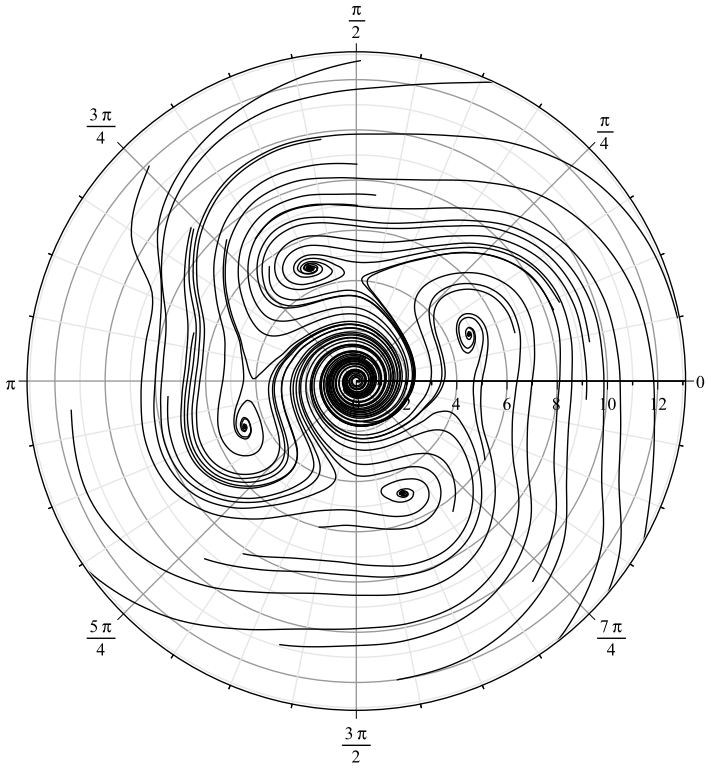

Figure 15: Experimental Van der Pol curves for n=4. The adimensioned amplitude is in mm/m. Parameters are: $n = 4$, $F_B = 51N$, $F_0 = -5.0N$, $f_{00} = 6.615Hz$, $\beta = 2.4\ 10^{-3}$, $L = 0.95m$, $k = 200\ 10^{-3}N/m$, $f_{exc} = 25.849813Hz$, $\rho_{00} = 0.976939$. The high number of decimal positions is to allow one to reproduce numerical results.

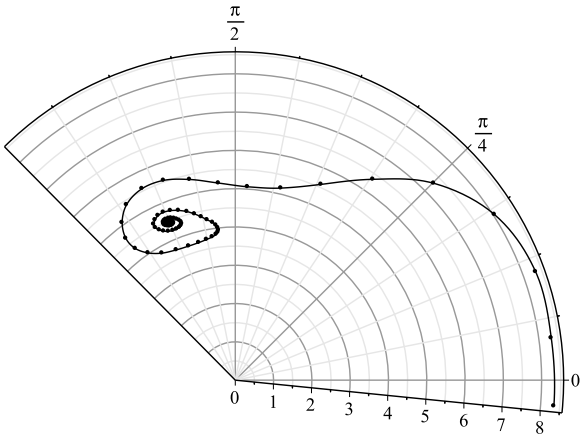

Figure 16: Detail of one curve from Fig. 15. There is one dot embedded on the curve every two periods of the beam's motion.

As can be seen in Fig. 17 (c) and (d), the point A's power spectrum components relative to the frequencies f_0 and 2 f_0 are kept respectively under 1.5 10^{-6} and 2 10^{-5}.

Fig. 18 gives numerical simulation results and experimental results relative to stationary regimes. Referring to [2,3], results of the numerical simulations on the averaged system (with smooth model) are given. The smooth model yields a curve with a crescent-shaped top part and a V-shaped bottom part, curve whose right part constitutes the stable stationary regimes, and the left part the unstable ones. Parameter values for the smooth model are the same as for Fig. 15, except $F_0 = -6.4N$. Other experimental results are also represented, with the same parameters as for Fig. 15 and various values of the excitation a_A. It can be seen that the experimental data are in good agreement with the smooth model in the whole region where experimental data are available. The "Model upper validity limit" as defined in [3] is outside the figure, which means that the smooth model is valid on the whole figure.

Fig. 19 shows that, for $n = 4$, and given the high sensitivity of the results against parameter values, the smooth model and the natural model are in good agreement with each other. It can be noticed that the skewed form of the V-shaped part of the stationary-solutions curve in the experimental data is better modeled by the natural model than by the smooth model, as can be seen in Fig. 19. This is due to a specific approximation in the smooth model, as explained in [3]. In conclusion, for $n = 4$, the experimental data are in good agreement with both the natural and the experimental models.

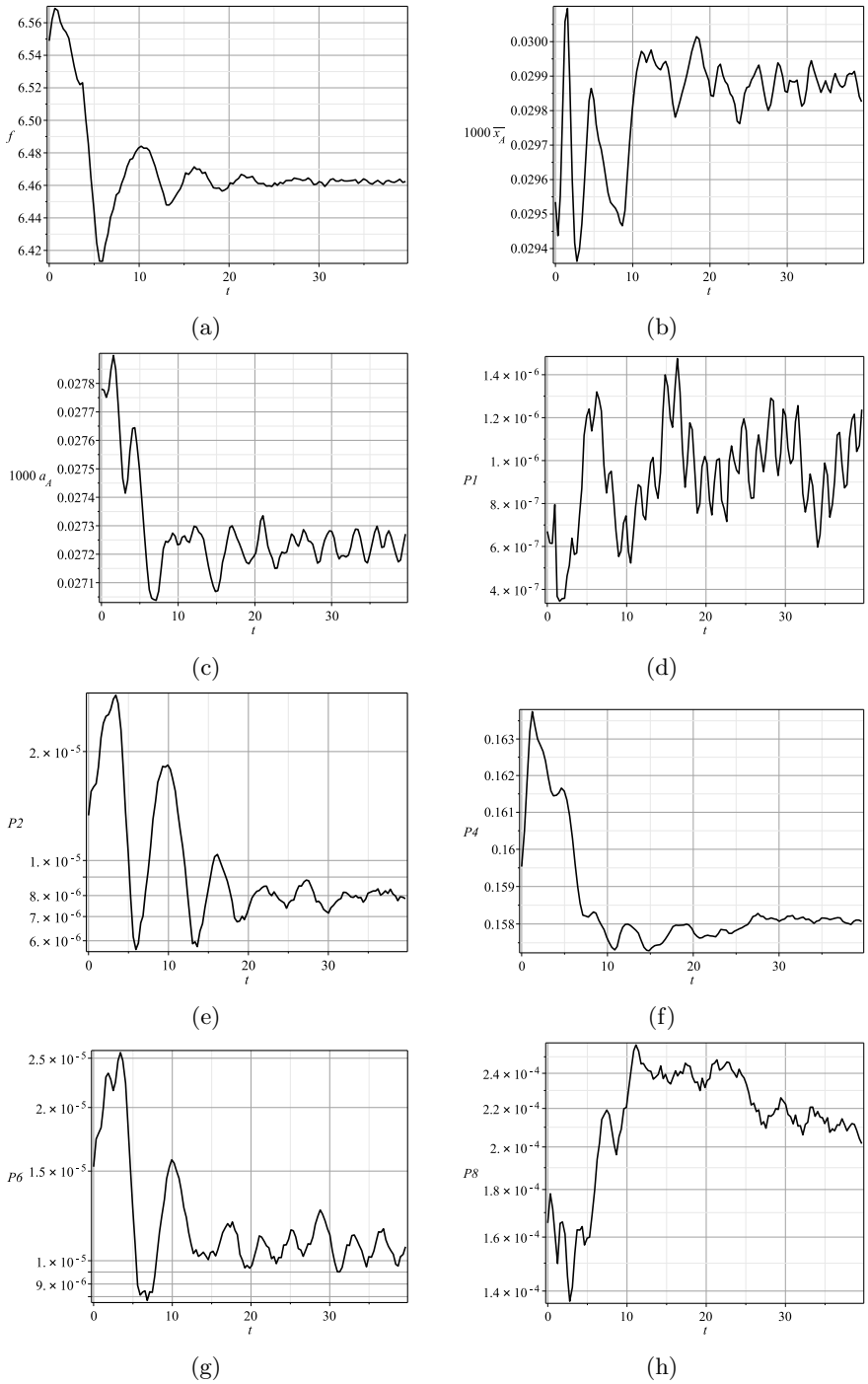

Figure 17: Details of the thread of Fig. 16: BUT frequency (BF) (a), point A's mean position (b), point A's amplitude (c), and point A's spectral components at: 1 x BF (d), 2 x BF (e), 4 x BF (f), 6 x BF (g), 8 x BF (h).

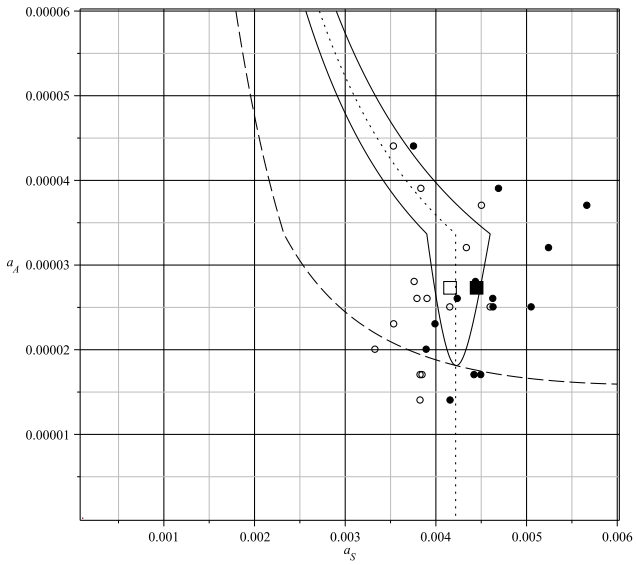

Figure 18: Stationary regimes, a_A (point A's amplitude) against a_S (stationary motion's amplitude) for $n = 4$. Comparison between smooth model and experimental results. The smooth model is represented as a solid line. The dashed line and the dotted line are the β-curve and the G-curve as described in [3]. The experimental results of Fig. 15 are represented as a solid square (stable point) and a hollow square (unstable point). Other stationary experimental points: unstable points (circles) and stable points (solid circles). The parameters are those of Fig. 15, except $F_0 = -6.4N$.

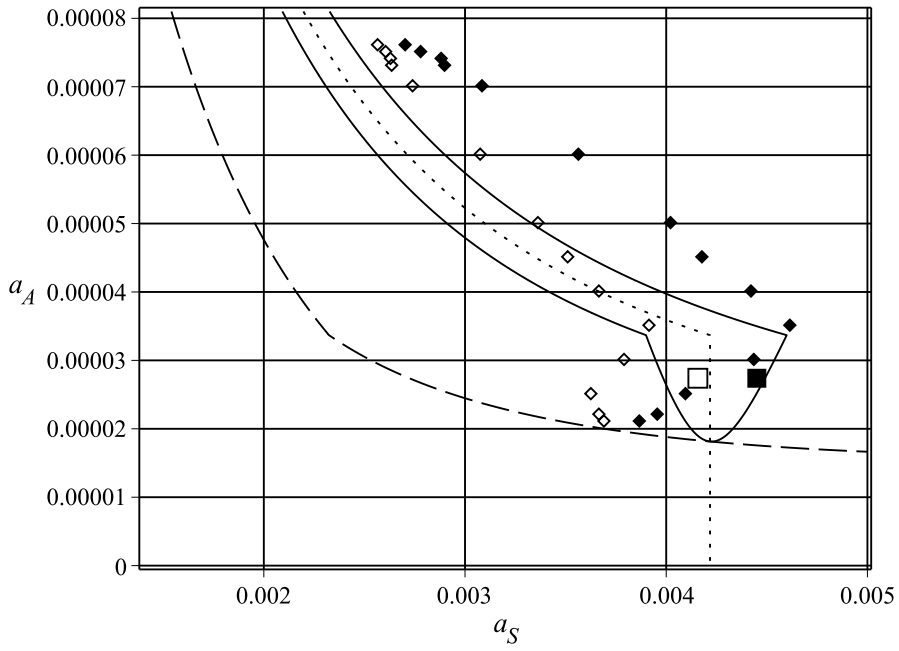

Figure 19: Stationary condition, a_A (point A's amplitude) against a_S (stationary motion's amplitude). Comparison between natural model (with second-order equation), represented as diamonds, and smooth model (with averaged system), represented as a solid line. The G-curve is the dotted line, while the β-curve is the dashed line. Parameters are those of Fig. 18. For the smooth model, stable and unstable stationary solutions are represented as an infinity of points belonging to solid lines, while for the natural model, a discrete series of stable (solid diamonds) and unstable (hollow diamonds) stationary points are represented.

4.2 Frequency ratio: $n = 6$

Fig. 20 shows the experimental Van der Pol curves obtained with a frequency ratio $n = 6$. Fig. 21 shows the detail of one curve from Fig. 20. This curve lasted for $60s$.

As can be seen in Fig. 22 (c) and (d), the shaker's components relative to

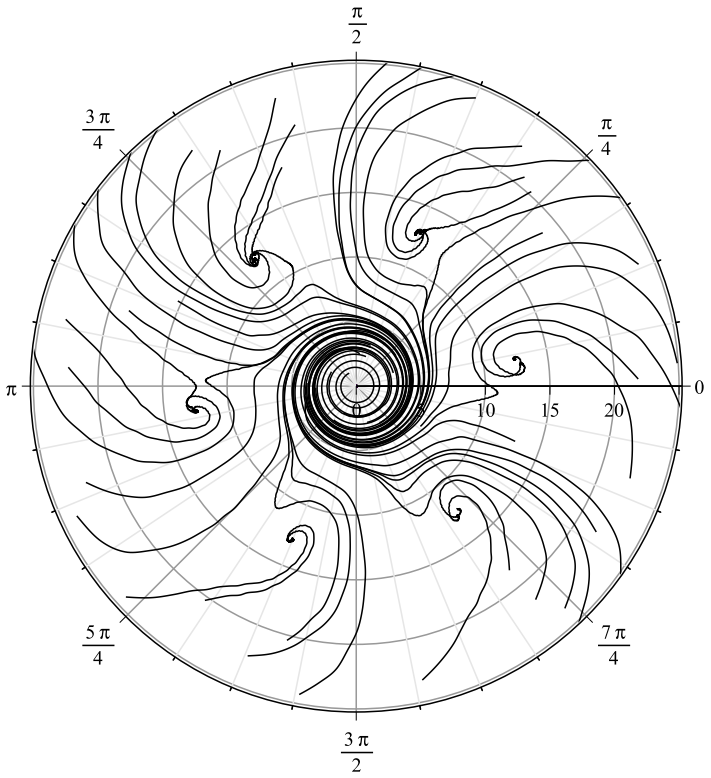

Figure 20: Experimental Van der Pol curves for n=6. The adimensioned amplitude is in mm/m. Parameter values are: $n = 6$, $\beta = 2.4\ 10^{-3}$, $F_B = 51N$, $F_0 = -5.0N$, $L = 0.95m$, $k = 130\ kN/m$, $f_{00} = 6.615Hz$, $f_{exc} = 39.500711Hz$, $\rho_{00} = 0.9952308$.

the frequencies f_0 and $2\ f_0$ are kept respectively under $3.5\ 10^{-5}$ and $1.6\ 10^{-5}$. Fig. 23 gives numerical simulation results and experimental results relative to stationary regimes. Referring to [2, 3], results of the numerical simulations on the averaged system (with smooth model) and results of numerical simulations on the second-order equation (using the natural model) are given. The smooth model yields a crescent-shaped curve whose right part is the stable regimes, and the left part the unstable regimes. Parameter values for natural and smooth model are the same as for Fig. 20, except $F_0 = -7.2N$. Experimental results

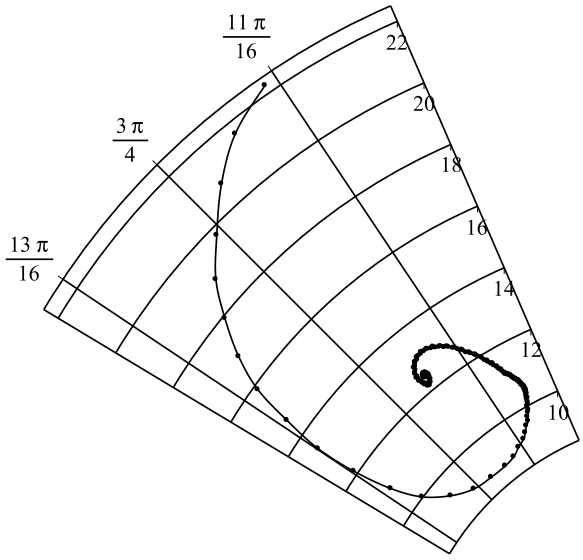

Figure 21: Detail of one curve from Fig. 20. There is one dot embedded on the curve every two periods of the beam's motion.

relative to Fig. 20 are also represented, along with other experimental results representing stable stationary regimes for the same parameters as for Fig. 20 and various values of the excitation a_A. In this last case (asterisk on Fig. 23), only stable stationary regimes are represented, because there were not enough experimental data to correctly identify the position of the unstable stationary representative points.

It can be seen that the agreement between experimental data and natural model is good, but that it is only fair between experimental data and smooth model. This is in all likelihood due to the approximations built into the smooth model and to the proximity to the vanishing of the argumental phenomenon for the parameters of Fig. 23. Indeed, the smooth model can be expected to be less performing when the truncated sinusoids used in [3] are about to vanish, due to the method employed to build the smooth model. However, given the sensitivity of the system to its parameters, the presence of the experimental data in the vicinity to the smooth model stationary-solutions curve can be considered a fair result.

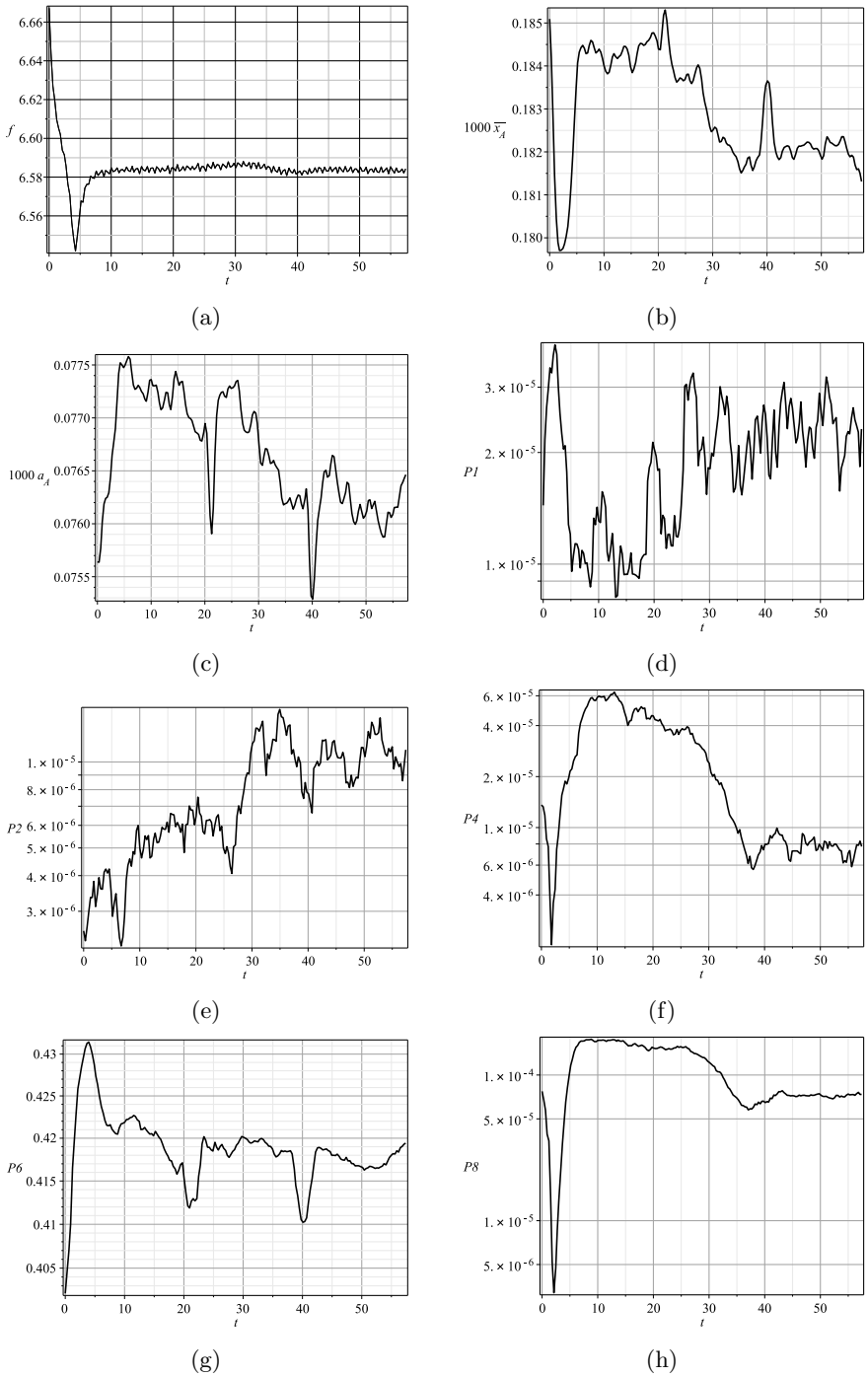

Figure 22: Details of the thread of Fig. 21: BUT frequency (BF) (a), point A's mean position (b), point A's amplitude (c), and point A's spectral components at: 1 x BF (d), 2 x BF (e), 4 x BF (f), 6 x BF (g), 8 x BF (h).

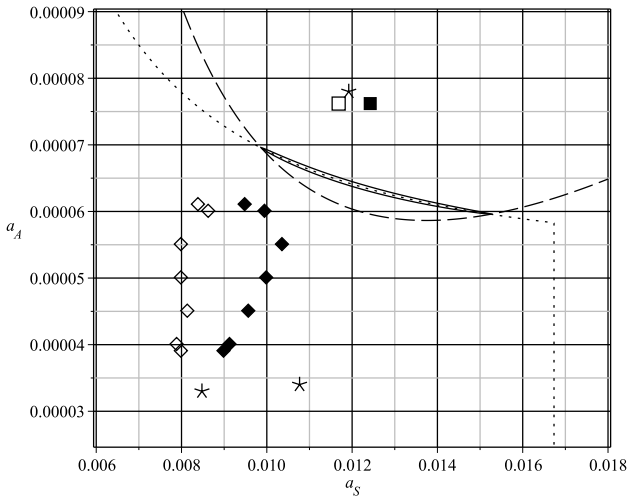

Figure 23: Stationary regimes, a_A (point A's amplitude) against a_S (stationary motion's amplitude) for $n = 6$. Comparison between models and experimental results. The smooth model is represented as a solid line. The dashed line and the dotted line are the β-curve and the G-curve as described in [3]. The natural model is represented as solid diamonds (stable points) and hollow diamonds (unstable points). The experimental results of Fig. 20 are represented as a solid square (stable point) and a hollow square (unstable point). Other experimental results (stable points only) are represented as asterisks.

5 Conclusion.

Experiments have been carried out with two beams placed head-to-head. The beam under test (BUT) was in a clamped-(clamped-guided) configuration. The second beam was controlled so as to provide an elastic intermittent contact with the BUT. It has been experimentally shown that a beam under test submitted to a harmonic axial excitation through an intermittent elastic contact can enter a stationary regime where its transverse vibration has a frequency which is the beam's fundamental frequency, and equal to a sub-multiple (other than one) of half the frequency of the axial excitation. The axial excitation was four or six times the fundamental frequency of the beam. These conditions constitute an argumental phenomenon.

In the case $n = 4$, the experimental data are in good agreement with both the natural and the smooth models. In the case $n = 6$, the experimental data are in good agreement with the natural model, and in fair agreement with the smooth model.

The experiments described herein have been carried out to the power limit of the shaker. To explore greater values of n, a more powerful shaker should be used. Also, lower values of the damping ratio could be employed. Finally, a more efficient device to convert the high-amplitude, low-force of the shaker into a low-amplitude, high-force excitation could be considered.

References

[1] M.J. Béthenod. Sur l'entretien du mouvement d'un pendule au moyen d'un courant alternatif de fréquence élevée par rapport à sa fréquence propre. *Comptes rendus hebdomadaires de l'Académie des sciences*, 207(19):847–849, November 1938. (in French).

[2] D. Cintra, G. Cumunel, and P. Argoul. A few properties in symbolic form for the argumental transverse vibration of a beam excited through permanent or intermittent elastic contact by a harmonic axial motion. *Journal to be determined*, 2017.

[3] D. Cintra, G. Cumunel, and P. Argoul. Modeling and numerical results for the argumental transverse vibration of a beam excited through permanent or intermittent elastic contact by a harmonic axial motion. *Journal to be determined*, 2017.

[4] Daniel Cintra and Pierre Argoul. Attractors capture probability in non-linear argumental oscillators. *Communications in Nonlinear Science and Numerical Simulation*, 48(Supplement C):150 – 169, 2017.

[5] Daniel Cintra and Pierre Argoul. Non-linear argumental oscillators: Stability criterion and approximate implicit analytic solution. *International Journal of Non-Linear Mechanics*, 94(Supplement C):109 – 124, 2017. A Conspectus of Nonlinear Mechanics: A Tribute to the Oeuvres of Professors G. Rega and F. Vestroni.

[6] Daniel Cintra and Pierre Argoul. Nonlinear argumental oscillators: A few examples of modulation via spatial position. *Journal of Vibration and Control*, 23(18):2888–2911, 2017.

[7] B. Cretin and D. Vernier. Quantized amplitudes in a nonlinear resonant electrical circuit. In *2009 Joint Meeting of the European Frequency and Time Forum and the IEEE International Frequency Control Symposium, vols 1 and 2*, volume 1 & 2, pages 797–800, Besançon, France, April 2009. Joint Meeting of the 23rd European Frequency and Time Forum/IEEE International Frequency Control Symposium.

[8] D. Doubochinski. *Argumental oscillations. Macroscopic quantum effects.* SciTech Library, August 2015.

[9] D.B. Doubochinski and J.B. Doubochinski. Amorçage argumentaire d'oscillations entretenues avec une série discrète d'amplitudes stables. *E.D.F. Bulletin de la direction des études et recherches, série C mathématiques, informatique*, 3:11–20, 1991. (in French).

[10] D. I. Penner, D. B. Duboshinskii, M. I. Kozakov, A. S. Vermel, and Yu. V. Galkin. Asynchronous excitation of undamped oscillations. *Phys. Usp.*, 16(1):158–160, 1973.

[11] Barun Pratiher and Santosha Kumar Dwivedy. Nonlinear response of a flexible cartesian manipulator withpayload and pulsating axial force. *Nonlinear Dynamics*, 57(1):177–195, Jul 2009.

[12] J.P. Treilhou, J. Coutelier, J.J. Thocaven, and C. Jacquez. Payload motions detected by balloon-borne fluxgate-type magnetometers. *Advances in Space Research*, 26(9):1423–1426, 2000.